Advances in Science and Technology Research Journal

Advances in Science and Technology Research Journal, 2025, 19(10), 80–93
https://doi.org/10.12913/22998624/207881
ISSN 2299-8624, License CC-BY 4.0

Received: 2025.05.19
Accepted: 2025.08.15
Published: 2025.09.01

Numerical procedure for investigating the water-added mass effect on the vibroacoustic characteristics of a cylindrical container

Artur Maurin[1]

[1] Institute of Fluid-flow Machinery PAS, Hydropower Department, ul. Fiszera 14 80-231 Gdansk, Poland
E-mail: amaurin@imp.gda.pl

ABSTRACT

Fluid-structure interaction (FSI) significantly influences the dynamic behaviour of submerged or fluid-containing structures. The "added mass" effect lowers natural frequencies and alters mode shapes. Understanding and accurately predicting this phenomenon is crucial for the design and safety assessment of various engineering systems, from offshore structures and storage tanks to hydraulic machinery. This paper presents a detailed numerical procedure, to investigate and quantify the added mass effect on the modal characteristics of a simple cylindrical container. The methodology for setting up the coupled fluid-structure problem, inherently capturing the inertial effects of the contained water, is described. The study validates the numerical approach against experimental results, showing frequency reductions of 24-33% due to added mass, with prediction errors for primary modes below 4%. This work establishes a reliable and validated FEM-based procedure for analysing vibroacoustic phenomena due to added mass, serving as an essential foundation for future analyses of such effects in more complex geometries, such as Francis turbine runners, where precise modal characterization is critical for operational dynamics and resonance avoidance.

Keywords: added mass, hydrodynamic mass, fluid-structure interaction (FSI), natural frequency shift, modal analysis, Ansys modal acoustics.

INTRODUCTION

The dynamic behaviour of structures immersed in or containing fluids is significantly influenced by fluid-structure interaction (FSI). A critical aspect of this interaction is the "added mass" or "hydrodynamic mass" effect, where the vibrating structure forces the surrounding fluid to accelerate, effectively increasing the structure's inertia [1, 2]. This added inertia lowers the structure's natural frequencies and can alter its mode shapes compared to vibrations in a vacuum or air. Accurately predicting these changes is paramount in various engineering fields, including marine engineering, aerospace (e.g., analysing water landing dynamics of specialized craft [3]), nuclear reactor design, civil infrastructure (e.g., storage tanks, dams), and critically, in hydraulic turbomachinery [4, 5]. Failure to account for added mass can lead to inaccurate resonance predictions, potentially causing fatigue damage or catastrophic failure.

Foundational analytical work, such as by Fritz [6], provided early calculation methods for idealized geometries. However, these analytical approaches often struggle with complex geometries, confined fluid domains, or the intricacies of flexible structural vibrations. Experimental investigations have therefore been crucial for understanding the phenomenon in real-world scenarios and for validating theoretical and numerical models. More specific studies on cylindrical structures,, Maheri and Severn [7], and Amabili et al. [8], have highlighted the complexities involved. Notably, Maheri and Severn [7] experimentally demonstrated that the added mass for flexible

cylinders is not constant but depends significantly on the vibration mode shape and frequency, deviating from simpler rigid-body assumptions, thereby underscoring the need for methods that capture the coupled system dynamics accurately. Techniques for identifying mass changes based on frequency shifts were also explored numerically for plates by Ostachowicz et al. [9], illustrating the sensitivity of modal parameters to inertial loading. The accurate determination of natural frequencies and mode shapes is fundamental in engineering design to prevent resonance and ensure structural integrity. Numerical methods, particularly the finite element method (FEM), are widely employed for such modal analyses across various disciplines [10]. These methods allow for the modelling of complex geometries and boundary conditions that are intractable analytically. Different FEM approaches exist, ranging from potential flow formulations to those solving the coupled acoustic wave equation for full Navier-Stokes equations using computational fluid dynamics (CFD) [11]. BEM has also proven effective, especially for external flow problems or radiation analysis [12, 13]. Numerical studies by Brandely and Lefrancois [14] investigated added mass effects in partially filled tanks using partitioned FSI schemes, highlighting numerical challenges and correction strategies. Research has also explored the frequency dependence of added mass and hydrodynamic damping [15], which can become important when fluid compressibility or viscosity plays a significant role, although often the inviscid, incompressible assumption provides a good approximation for the inertial effect at lower frequencies.

While foundational analytical and experimental studies on simple geometries have established the principles of added mass, accurately predicting these effects for industrially relevant components with complex shapes remains a significant challenge. This paper focuses on applying a modern, FEM-based acoustic FSI simulation approach, specifically using the Ansys Modal Acoustics module, to investigate the added mass effect on a fundamental structural element: a water-filled cylindrical container (the glass). This geometry, while simple, captures essential FSI characteristics relevant to many engineering applications like tanks and pipes, and serves as a crucial validation case due to the availability of comparative experimental and analytical data [8, 10]. The numerical approach inherently couples the structural dynamics with the fluid acoustics (wave equation), allowing for the direct calculation of the modified natural frequencies and mode shapes of the coupled system, thus implicitly capturing the added mass effect without resorting to simplified coefficients.

The primary motivation for this study comes from the need for reliable numerical procedures to analyse more complex geometries of turbomachinery components, specifically modern Francis turbine runners. Experimental work by Rodriguez et al. [4] and Cao et al. [6] has confirmed that added water mass significantly reduces the natural frequencies of runners, impacting their operational safety and susceptibility to resonance. Furthermore, numerical studies like Wang et al. [16] have shown that added mass not only shifts frequencies but can also alter the complex mode shapes of turbine runners, although this particular result primarily stems from simulation and awaits broader experimental confirmation for various mode shapes. Given the intricate geometry and demanding operational environment of these runners, accurate prediction of added mass effects through validated numerical simulation is essential for design and analysis. The scientific contribution of this work is the development and experimental validation of a specific numerical procedure for assessing the water-added mass effect on structural acoustics using Ansys Modal Acoustics. This study, for the first time details the methodology for a fluid-filled cylindrical container, demonstrating the tool's capability to accurately predict frequency reductions and mode shape changes. This validated approach, provides a reliable and foundational numerical framework for tackling similar FSI phenomena in more complex engineering systems, such as hydraulic turbines, where precise modal characterization is crucial.

GOVERNING EQUATIONS

The numerical investigation is performed using the Ansys Workbench environment, employing the prestressed Modal Acoustics analysis system. This system is designed to compute the modal parameters (natural frequencies and mode shapes) of a structure coupled with a contained or surrounding acoustic fluid domain, inherently accounting for the fluid loading effects, including added mass. The structural vibration influences the fluid pressure field, and the fluid pressure field exerts forces

(including the inertial force related to added mass and damping forces) back onto the structure.

Fluid-structure interaction added mass

When a structure vibrates while in contact with a fluid (like water), it has to displace the fluid as it moves. According to Newton's laws, accelerating this fluid requires a force. From the structure's perspective, this force feels like an additional inertia or mass that resists its motion. This is the **"**added mass" or "hydrodynamic mass". The primary effect of added mass is to lower the natural frequencies of the structure compared to its vibration in a vacuum or air (which has negligible added mass). The mode shapes can also be altered, sometimes significantly.

The analysis solves the coupled acoustic-structural eigenvalue problem, using specific acoustic fluid elements (e.g., FLUID30, FLUID220, FLUID221 in APDL; corresponding elements in Workbench Acoustics). These elements discretize the acoustic wave equation using pressure as the primary degree of freedom (DOF) at the nodes.

Coupled vibroacoustic analysis

The analysis within the Ansys modal acoustics system solves a coupled vibroacoustic eigenvalue problem to determine these modified modal characteristics. The structural domain is discretized using standard finite elements, governed by the structural equation of motion. The fluid domain, assumed to be an acoustic fluid (inviscid, compressible, with small disturbances), is discretized using acoustic finite elements, governed by the acoustic wave equation.

At the fluid-structure interface, appropriate continuity conditions ensure that the structural motion influences the fluid pressure, and conversely, the fluid pressure exerts forces back onto the structure. This two-way coupling is fundamental to accurately capturing the FSI phenomena, including the added mass effect. The Ansys software formulates a fully coupled system matrix that combines the structural degrees of freedom (displacements) and the fluid degrees of freedom (acoustic pressure). Solving the eigenvalue problem for this coupled system directly yields the natural frequencies and mode shapes of the combined structure-fluid system. The added mass effect is thus implicitly included in this formulation without the need to calculate an explicit added mass matrix.

For a detailed mathematical description of the finite element formulations for the structural and acoustic domains, the coupling matrices, and the solution of the coupled eigenvalue problem as implemented in Ansys, readers are referred to the relevant sections of the Ansys online Theory Reference [17].

MODEL PREPARATION

The numerical simulations were performed using the ANSYS Workbench environment (Version 2024 R1), primarily employing the Modal Acoustics analysis system, which couples structural mechanics with fluid acoustics to solve for the modal parameters of the fluid-structure interaction (FSI) system.

Model geometry and materials

The 3D geometry for the numerical simulation was created using the ANSYS SpaceClaim environment. It accurately represents the features of cylindrical container used in the experimental setup, including its precise dimensions (radius, height, wall thickness). To define the computational domain for the fluid and facilitate the application of boundary conditions, the container geometry was enclosed within a larger domain (here, a sphere). For simulations involving a free surface (like water partially filling the glass), the fluid domain was partitioned to explicitly represent this interface (Figure 1).

Material properties were assigned to the respective domains based on the physical components involved. The properties for the fluids (air and water) and the structure (glass) used in the simulations are detailed in Table 1 and Table 2, respectively.

For the fluid domains, modelled using acoustic physics within the Modal Acoustics framework, the essential material properties required are the density (ρ) and the speed of sound (c), as listed in Table 1. Fluid density determines the inertial properties of the fluid, which is fundamental to the added mass effect. The speed of sound governs the fluid's compressibility and the propagation speed of acoustic pressure waves within it, which dictates the fluid's acoustic stiffness contribution and coupling behaviour. While viscosity is also listed in Table 1 for completeness, it is generally neglected in standard acoustic

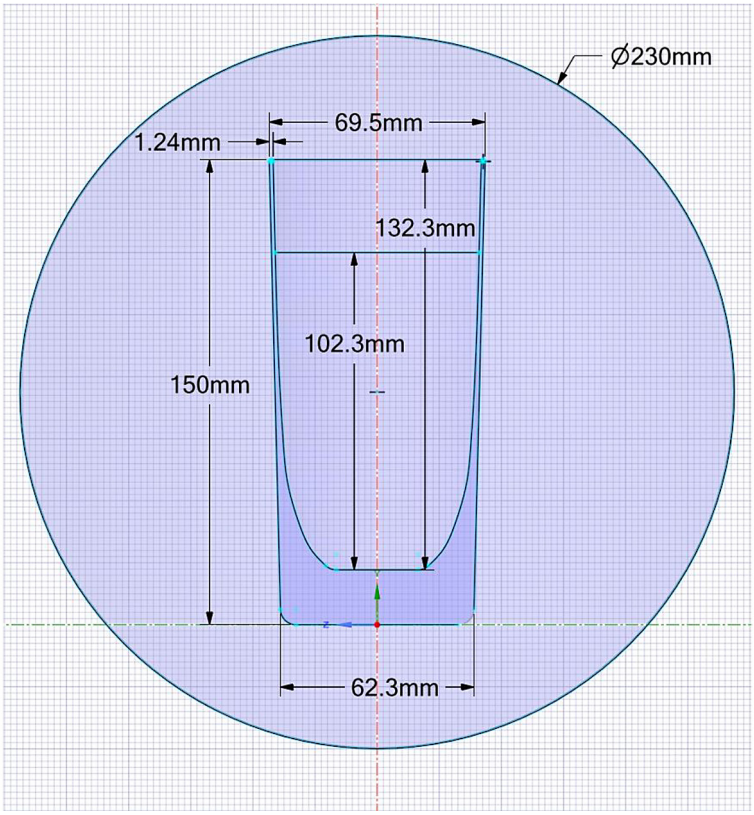

Figure 1. The cross-section of enclosed container geometry

fluid formulations used in Modal Acoustics, which solve the inviscid wave equation.

For the structural domain (the glass), the mechanical properties relevant to modal analysis are its elastic properties and density (ρ_s), as provided in Table 2. Specifically, Young's Modulus (E) and Poisson's Ratio (v) define the material's stiffness, governing the structural stiffness matrix [K_s], while the density (ρ_s) determines the structural inertia, governing the structural mass matrix [Ms]. These properties dictate how the solid structure deforms and vibrates. Other properties listed in Table 2, such as thermal properties or strength limits, are not directly used in the linear elastic modal analysis performed here. Notably, the speed of sound within the *glass* material is not required for this type of structural modal analysis. This is because the analysis focuses on the macroscopic vibration of the structure based on its elastic deformation (governed by E, v) and inertia (governed by ρ_s), rather than modeling the propagation of acoustic waves *through* the solid material itself. The acoustic properties are only essential for the domain explicitly modelled using acoustic elements (i.e., the fluid).

Meshing strategy

Geometry bodies/volumes for the structure and the fluid domain(s) (either surrounding the structure or contained within it) are created with the respect to geometrical details. The surface representing the fluid-structure interface must be perfectly conforming. In Ansys for this type of coupled vibroacoustic simulation. For the structural domain (the cylindrical container), 3D solid elements such as SOLID187 (higher-order 3D 10-node tetrahedral solid element) was employed to accurately capture its deformation. For the acoustic fluid domain (the water), acoustic elements such as FLUID221 (higher-order 3D tetrahedral 10-node acoustic fluid element) were used to adapt for the complicated geometry. These acoustic elements are formulated with pressure as the primary degree of freedom. The acoustic-structure interaction (ASI) region in Ansys automatically handles the coupling between the structural displacement DOFs and the fluid pressure DOFs at the shared interface. The choice of higher-order elements is generally preferred for improved accuracy in capturing stress gradients and curved geometries. Crucially, the mesh must be conformal at the FSI interface, meaning nodes are shared between the structural surface

Table 1. Acoustic fluid material properties

Property	Air	Water	Unit
Density	1.225	998.2	kg/m^3
Speed of sound	346.25	1482.1	m/s
Viscosity	1.789E-05	0.001003	kg/ms

Table 2. Mechanical material properties of glass

Property	Value	Unit
Density	2250	kg/m^3
Young's modulus	64	GPa
Poisson's ratio	0.155	-
Bulk modulus	30.918	GPa
Shear modulus	27.706	GPa
Tensile yield strength	28	MPa
Tensile ultimate strength	160	MPa

and the fluid surface. Alternatively, contact-based connections can sometimes be used, but conformal meshing is often preferred for modal analysis. The "Acoustic" physics region was assigned to the fluid body, while the "Structural" physics region was assigned to the solid body. An acoustic-structure interaction region was defined at the shared interface surface(s) and designated as the FSI boundary. Ansys automatically links the structural and acoustic physics at this interface.

A mesh convergence study was performed to ensure the accuracy and efficiency of the finite element model used for the modal analysis. Several mesh sizes were evaluated: five homogeneous meshes with increasing element counts (approximately 11k, 15k, 21k, 36k, 66k, and 150k elements) – reaching convergence at 66k (Figure 2) and one mesh adapted to geometric curvature (approximately 51k elements). The natural frequencies obtained for the first 32 modes (16 unique modes) were compared across with 150k mesh (Figure 3).

The results for the homogeneous meshes demonstrate clear convergence, with the calculated natural frequencies stabilizing as the element count increases from 11k towards 150k elements. The 150k element mesh, being the most refined, is considered to provide the reference solution for the homogeneous meshing strategy.

A comparison was then made between the curvature-adapted mesh (51k elements) and the homogeneous meshes. For the lower and mid-range modes (approximately Modes 1–28), the frequencies obtained with the 51k adapted mesh (Figure 4) showed excellent agreement with those from the most refined 150k homogeneous mesh, with differences generally well below 1% and only increasing slightly for the higher modes in this range. For example, for Mode 10, the 51k adapted mesh yielded 5279.6 Hz compared to 5258.8 Hz from the 150k mesh (difference ≈ 0.4%, Figure 3).

Crucially, the 51k adapted mesh achieved this level of accuracy with significantly fewer elements than the most refined homogeneous meshes (150k or even 66k). When compared to the 66k homogeneous mesh, the 51k adapted mesh consistently provided results closer to the 150k reference frequencies, despite having ~23% fewer elements. This clearly demonstrates that adapting the mesh density based on geometric curvature is a substantially more efficient approach than uniformly increasing the density of a homogeneous mesh, yielding high accuracy at a lower computational cost for most modes. Based on this validation, the 51k element mesh adapted to curvature was selected for subsequent analyses presented in this paper, as it offers an optimal balance between high accuracy for the primary modes of interest and computational efficiency. The potential limitations for resolving very high-frequency modes with this specific adapted mesh are acknowledged.

Structural boundary conditions

Constraints were applied to the structural domain to represent its physical support. For instance, a 'Fixed Support' condition was applied to the base of the cylinder to simulate clamping or rigid mounting, matching the experimental setup. Symmetry conditions were used where applicable to reduce model size.

Fluid domain boundary conditions

FSI interface

The interaction between the fluid and the structure at the wetted surfaces was defined using the Acoustic-Structure Interaction condition available in Ansys Workbench. This condition automatically couples the pressure degrees of freedom in the fluid elements with the displacement degrees of freedom in the structural elements, enforcing continuity of normal velocity and forces across the interface. This coupling inherently incorporates the added mass and fluid loading effects.

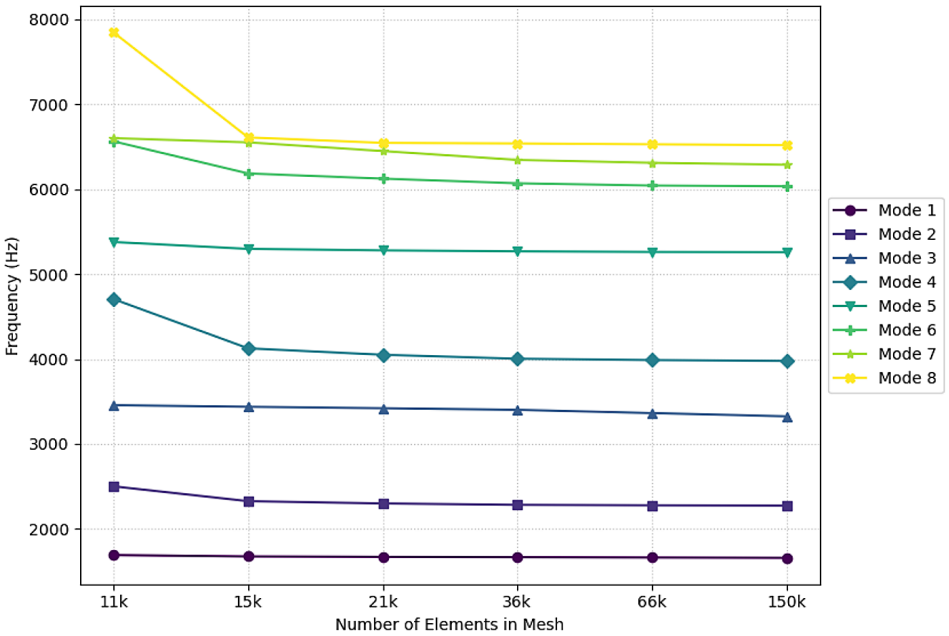

Figure 2. Convergence of natural frequencies with increasing mesh density

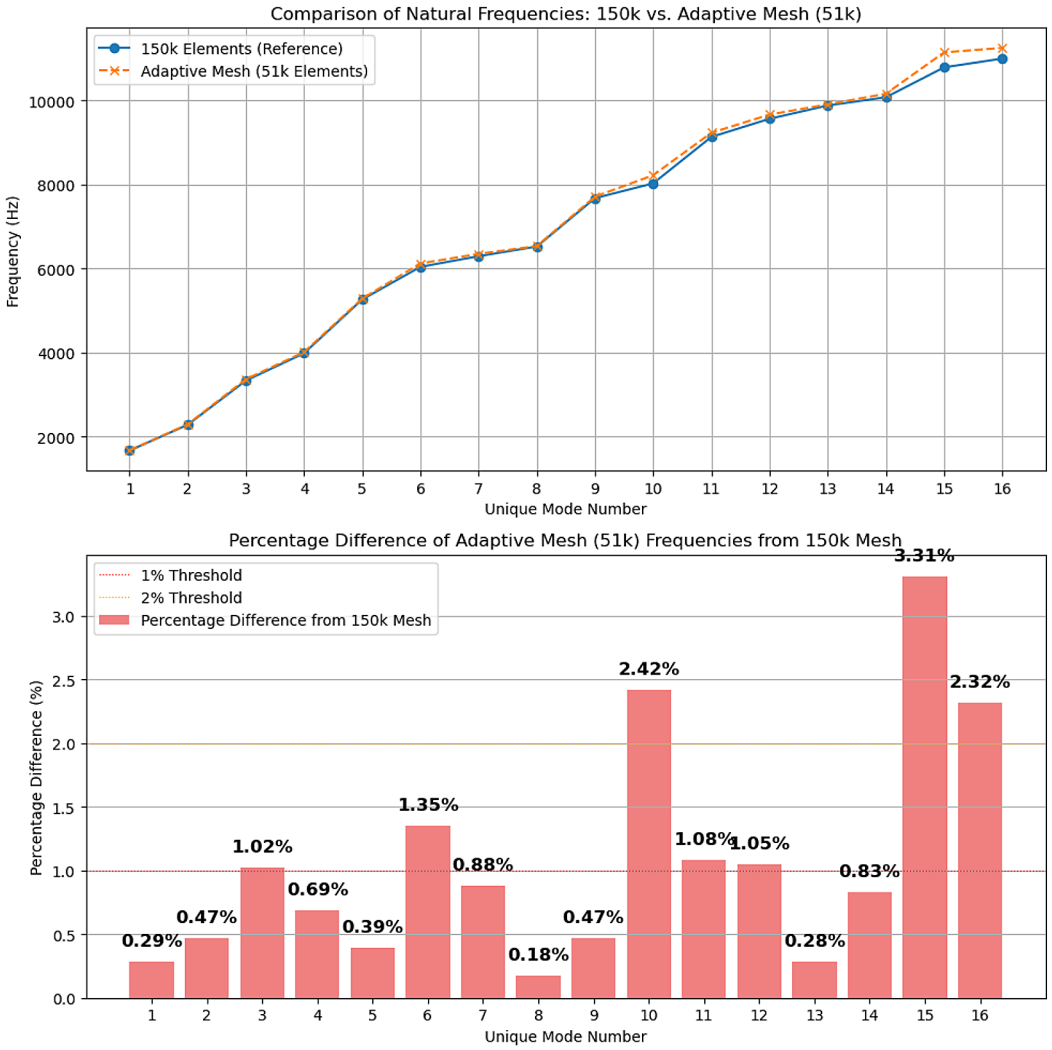

Figure 3. Comparison of high resolution homogeneous mesh vs adaptive mesh

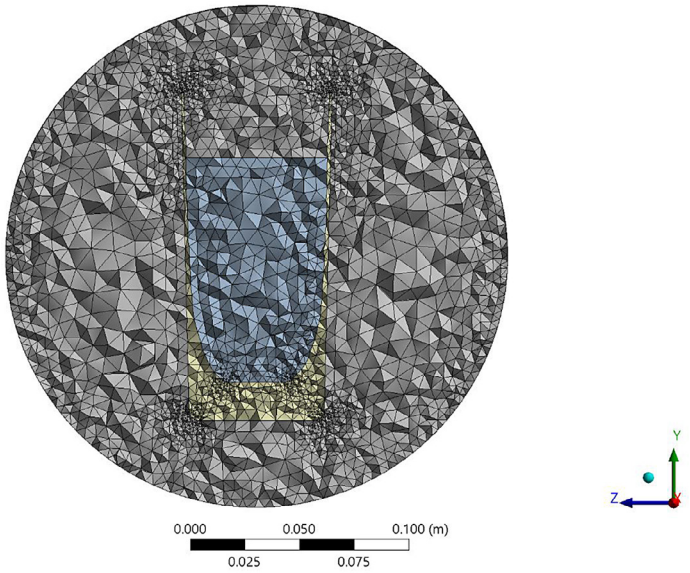

Figure 4. The cross-section of mesh with variable density around geometry curvature

Contained fluid boundaries

For the fluid contained within the cylinder, the FSI interface defined above serves as the primary boundary condition at the walls and base.

Free surface

The top surface of the water, open to the air, was modelled using a Pressure Release boundary condition (Pressure P= 0). This simulates a free surface where acoustic waves reflect with a phase change, appropriate for neglecting surface tension and the mass/impedance of the air above.

Open Domains

For problems involving structures submerged in large or infinite fluid domains (not the current case), appropriate non-reflecting boundary conditions such as Impedance boundaries ($Z = \rho f\, c$), Radiation boundaries, or perfectly matched layers (PMLs) would be necessary on the far-field fluid boundaries to simulate wave propagation away from the structure.

Fluid-structure coupling

As mentioned, the Acoustic-Structure Interaction condition manages the coupling at the shared interface, forming the core of the FSI simulation.

Hydrostatic prestress

For structures subjected to significant static fluid pressure (e.g., tall tanks or submerged components under high pressure like turbine runners), the resulting pre-stress state can influence the structural stiffness and thus the natural frequencies. While potentially negligible for a shallow glass of water, this effect can be included in Ansys via a two-step workflow:

- A static analysis (either structural or coupled acoustic-structural) is performed first to calculate the stress distribution in the structure due to the static pressure load (e.g., hydrostatic pressure $P = \rho f\, g$ applied to wetted surfaces).
- The subsequent modal acoustics analysis is then configured to include these prestress effects. Ansys calculates a stress stiffness matrix [Kσ] from the static results and adds it to the structural stiffness matrix [K_s], solving the eigenvalue problem for the effective stiffness [Keffective] = [K_s] + [K_σ] . This accounts for stress stiffening or softening phenomena.

Water detachment (cavitation) and critical conditions

Cavitation occurs when the absolute pressure in the liquid drops below its vapour pressure at the prevailing temperature. During vibration, the dynamic pressure fluctuations (P) are superimposed on the static pressure (*Hydrostatic*). If $Hydrostatic + P < P_{vapour}$, bubbles of vapor can form. This happens when the negative pressure swing caused by the structure vibrating *outward* (pulling away from the fluid) is large enough to overcome the static ambient

pressure plus the liquid's tensile strength (often negligible) and reach the vapour pressure. This requires sufficiently high vibration amplitude/velocity at a given frequency. When cavitation occurs, the water effectively detaches from the structure locally. The fluid boundary condition changes drastically: instead of resisting motion (added mass), there's a near-vacuum (vapour bubble) offering little resistance. This is a highly non-linear effect. It fundamentally changes the added mass and damping at that location, altering mode shapes and frequencies, often introducing significant damping and limiting vibration amplitude.

Standard Ansys Modal Acoustics generally does not account for cavitation as an inherently *linear* technique. It assumes small perturbations and that the material properties (including fluid properties and the FSI coupling) remain constant regardless of vibration amplitude. Cavitation is a threshold phenomenon and highly non-linear. The effective fluid properties and boundary conditions change dramatically and depend on the vibration amplitude reaching the cavitation threshold. While static prestress accounts for the effect of a static pressure field on stiffness, it doesn't capture the dynamic pressure drops needed to trigger cavitation during the vibration cycle itself. Due to this limitation the overcritical conditions is beyond the scope of this study.

NUMERICAL ANALYSIS RESULTS

Numerical simulations were performed using three separate setups in ANSYS to understand the influence of fluid loading and potential prestress (PS) effects:

- Modal: Standard modal analysis of the glass structure in vacuum (representing air for negligible air loading).
- PS Modal Acoustic AIR: Pre-stressed modal acoustics analysis with the glass surrounded by air (modelled as an acoustic fluid), assuming negligible prestress from air. This serves primarily as a baseline check for the acoustic coupling setup.
- PS Modal Acoustic WATER: Pre-stressed modal acoustics analysis with the glass filled with water (modeled as an acoustic fluid), simulating the FSI condition. Prestress effects from hydrostatic pressure were considered negligible for this geometry and fill level.

The calculated natural frequencies (FR) and corresponding mode shape orders (designated by Nodal Diameter, ND) for the first ~24 modes are presented in Table 3. The mode shapes of PS Modal Acoustic WATER (Figure 5), listed by frequency are additionally visualised in Appendix.

EXPERIMENTAL VERIFICATION

To validate the numerical simulations, experimental modal analysis was performed on the physical glass container. A piezoelectric sensor was mounted near the base of the container using a custom 3D printed clamp designed to ensure consistent positioning and minimal interference, as shown in Figure 6.

The container was tested in two conditions: empty (representing the 'Air' case) and filled with water to the same level simulated numerically. Vibration was induced (likely via impact excitation, inferred from the spectral results shown later) and the resulting acceleration signal was captured and processed using an FFT analyser (Rigol DHO804 oscilloscope) to identify resonant frequencies. Vibration was induced via impact hammer excitation to ensure a broadband energy input suitable for exciting the structural modes of interest. The signal was acquired with a sampling rate of 625 MSa/s which is well above the Nyquist frequency for the anticipated structural modes (up to several kHz), ensuring accurate waveform capture without aliasing while managing data volume. The oscilloscope's maximum available record length (50 Mpts per acquisition) was utilized to maximize the frequency resolution of the subsequent FFT analysis. For each impact, an edge trigger was set on the accelerometer channel, with the trigger level carefully adjusted to be slightly above the ambient noise floor to reliably capture the transient response. "Normal" trigger mode was employed to acquire data from single impact events. Post-processing of the acquired time-domain data was performed using the DHO804's built-in FFT capabilities. Prior to performing the FFT, a Hanning window was applied to each captured time-domain response to minimize spectral leakage. To enhance the signal-to-noise ratio (SNR) and obtain clear, stable frequency spectra, spectral averaging was conducted. For each test condition (empty and water-filled container), 10 individual impact measurements were performed, and their corresponding spectra were averaged. The natural frequencies

Table 3. List of mode shapes (MS), their natural frequencies (FR) and designated MS order

Modal analysis			PS modal acoustic AIR			PS modal acoustic WATER		
MS nr [-]	FR [Hz]	MS order	MS nr [-]	FR [Hz]	MS order	MS nr [-]	FR [Hz]	MS order
1	1664.8	2ND1	1	640.6	0ND1	1	924.91	0ND
2	1664.9	2ND1	2	849.81	0ND2	2	1159.8	2ND1
3	2285.6	3ND1	3	1224.2	1ND1	3	1159.9	2ND1
4	2285.7	3ND1	4	1224.2	1ND1	4	1223.2	1ND1
5	3358.6	1ND1	5	1655.8	2ND1	5	1223.2	1ND1
6	3362.3	1ND1	6	1656.1	2ND1	6	1715.2	3ND1
7	4005.2	4ND1	7	1825.1	0ND3	7	1715.3	3ND1
8	4006.1	4ND1	8	1899.5	0ND4	8	1745.9	0ND2
9	5279	3ND2	9	2075.5	1ND2	9	2072.3	1ND2
10	5279.6	3ND2	10	2075.6	1ND2	10	2072.4	1ND2
11	6114.1	4ND2	11	2276.2	3ND1	11	2150.6	1ND3
12	6117.3	4ND2	12	2276.3	3ND1	12	2151.6	1ND3
13	6343.5	5ND1	13	2468.8	2ND2	13	2210.4	0ND3
14	6343.8	5ND1	14	2468.8	2ND2	14	2467.3	2ND2
15	6530.1	2ND2	15	2784.7	0ND5	15	2467.4	2ND2
…	…	…	…	…	…	…	…	…
20	9225.7	6ND1	20	2995.5	2ND3	20	2985.8	0ND4
21	9226.9	6ND1	21	3031	3ND2	21	3002.3	0ND5
22	9657.2	4ND3	22	3044.8	3ND2	22	3011.3	0ND5
23	9662.5	4ND3	23	3044.9	1ND4	23	3016.3	4ND1
24	9903.6	3ND3	24	3155.7	1ND4	24	3017.5	4ND1
…	…	…	…	…	…	…	…	…
			43	3990.3	4ND1	63	4721.9	5ND1
			44	3991.1	4ND1	64	4725.4	5ND1
			…	…	…	…	…	…
			132	6318.8	5ND1			
			133	6319.8	5ND1			
			…	…	…			

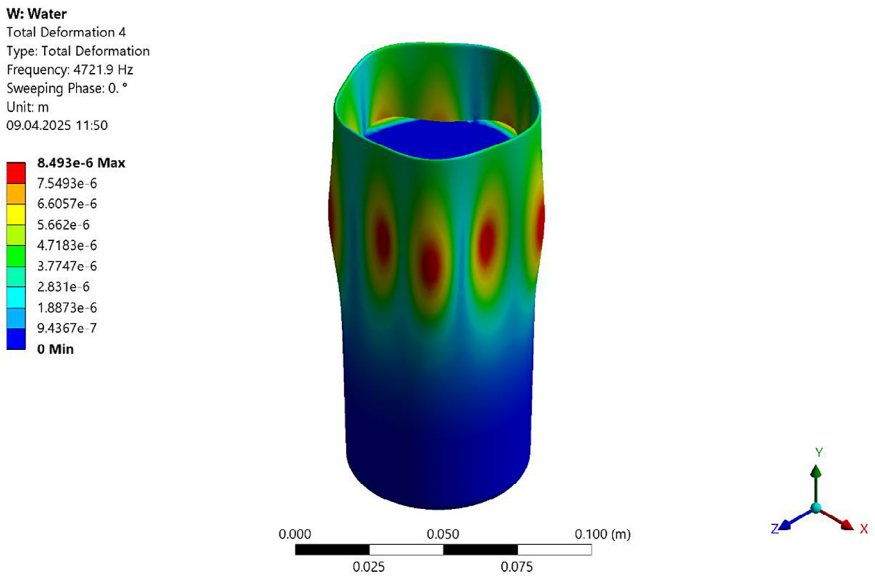

Figure 5. 5ND1 mode shape of cylindrical container filled with water at 4721.9 Hz

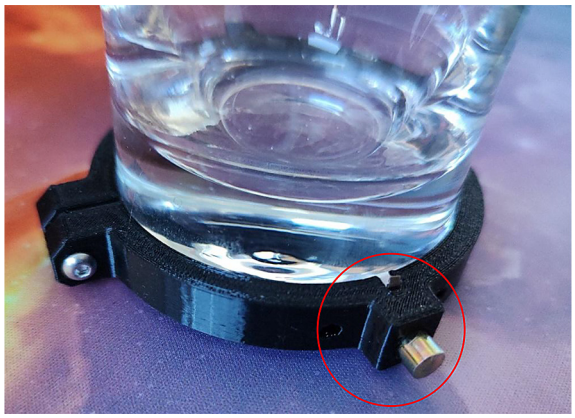

Figure 6. 3D printed clamp for the piezoelectric sensor

of the container were then identified by picking the peaks from the resulting averaged magnitude spectra. The primary measured natural frequencies for both conditions are listed in Table 4, along with an 'Equivalent Nodal Diameter' (EQ) designation based on comparison with expected shell vibration patterns and the numerical results.

A direct comparison between the measured frequencies (Table 4) and the simulated frequencies from the 'PS Modal Acoustic WATER' analysis (Table 3, summarized in Table 5) shows reasonable agreement, particularly for the lower-order modes.

- 2ND1 Mode: Measured at 1705.9 Hz (Air) and 1147.5 Hz (Water), giving a 32.7% reduction. The simulation predicted 1656 Hz (Air) and 1160 Hz (Water), a 29.9% reduction. The error in simulated frequency is approximately -3% (Air) and +1% (Water).
- 3ND1 Mode: Measured around 2246-2347 Hz (Air) and 1703–1721 Hz (Water), average reduction ~25%. Simulation predicted 2276 Hz (Air) and 1715 Hz (Water), reduction 24.6%. Errors are roughly +1% (Air) and ±0% (Water).
- 4ND1 Mode: Measured around 3931–3961 Hz (Air) and 2905 Hz (Water), average reduction ~26.5%. Simulation predicted 3991 Hz (Air) and 3017 Hz (Water), reduction 24.4%. Errors are roughly +1% (Air) and +4% (Water).

Higher modes show larger discrepancies or were difficult to definitively match between experiment and simulation based solely on frequency, highlighting the complexity of modal identification in coupled systems. Figure 7 visually confirms the frequency reduction effect observed experimentally. It shows overlaid FFT spectra obtained from the measurements. The peaks corresponding to the natural frequencies of the empty container (yellow-pink trace) are clearly shifted to lower frequencies when the container is filled with water (green-blue trace), consistent with the added mass phenomenon.

COMPARISON OF NUMERICAL AND EXPERIMENTAL RESULTS

To facilitate a direct comparison between the numerical predictions and experimental

Table 4. List of measured frequencies (FR) with equivalent (EQ) nodal diameter (ND) order designation

FR nr [-]	Measurement air		Measurement water	
	[Hz]	order EQ	[Hz]	order EQ
1	1705.93	2ND1	1147.46	2ND1
2	1705.--	2ND1	1147.--	2ND1
3	2246.09	3ND1	1223.75	1ND1
4	2346.80	3ND1	1263.42	1ND1
5	3930.66	4ND1	1702.88	3ND1
6	3961.18	4ND1	1721.19	3ND1
7	5725.09	-	2349.85	2ND2
8	6152.34	5ND1	2349.--	2ND2
9	6152.--	5ND1	2905.27	4ND1
10	6478.88	-	2905.--	4ND1
11	6521.60	-	3961.18	-
12	6564.32	-	6484.98	-
13	9317.01	6ND1	8886.71	-
14	9317.--	6ND1	9158.32	-

measurements, the results were filtered and processed. Specific mode orders predicted by the simulation, namely those with Nodal Diameters (ND) of 0 and 1 (0NDx, 1NDx), as well as certain higher-order or complex modes (3ND2, 2ND2, 6ND1), were excluded from this direct comparison table.

The 0ND ('breathing') and 1ND ('swaying' or 'beam') modes often involve significant uniform radial motion or overall axial/torsional displacement of the cylinder. It is likely that the experimental setup, utilizing a piezoelectric sensor positioned radially near the base, was not optimally configured or sufficiently sensitive to clearly excite and capture these specific mode types, which explains their apparent absence in the measured frequency peaks listed in Table 4.

Furthermore, matching higher-order modes (like 2ND2, 3ND2, 4ND3 etc.) between the comprehensive list predicted by simulation (Table 3) and the limited peaks strongly excited or clearly measurable in the experiment (Table 4) becomes increasingly challenging. This is due to factors such as the higher density of modes at higher frequencies, potential mode shape complexity, and limitations in experimental excitation and measurement resolution.

Therefore, the comparison focuses on the lower-order circumferential bending modes (ND $\geq$ 2) that were clearly identifiable in both datasets. For doublet modes (pairs with the same ND designation and nearly identical frequencies predicted by simulation or measured experimentally), the frequencies were averaged to represent the single physical mode.

Table 5 presents this direct comparison, including the calculated percentage error of the simulation relative to the experimental results and the FRR due to water, calculated as

$$FRR = (FrAir - FrWater) / FrAir \quad (1)$$

As shown in Table 5, there is reasonable quantitative agreement between the simulated and experimental frequencies, particularly for the lowest bending modes (2ND1 and 3ND1). The percentage errors for these modes are within ±3% for air and approximately ±1% or less for water. The agreement slightly decreases for the 4ND1 mode, with errors up to ~4% in water. The 5ND1 mode was clearly measured in air but could not be reliably identified in the water measurements.

The FRR due to water also show good qualitative agreement, with both simulation and experiment indicating substantial reductions (ranging from ~24% to ~33%) for these modes. The quantitative differences in FRR reflect the underlying discrepancies in the absolute frequency predictions.

The experimental results validate the numerical model's ability to capture the fundamental physics of the added mass effect (Figure 8), showing significant frequency reductions due to water loading that are broadly consistent with simulation predictions, especially for lower-order modes.

DISCUSSION

The numerical and experimental results presented consistently demonstrate a significant reduction in the natural frequencies of the cylindrical container when filled with water, confirming the presence of a substantial added mass effect. The observed FRR, ranging from

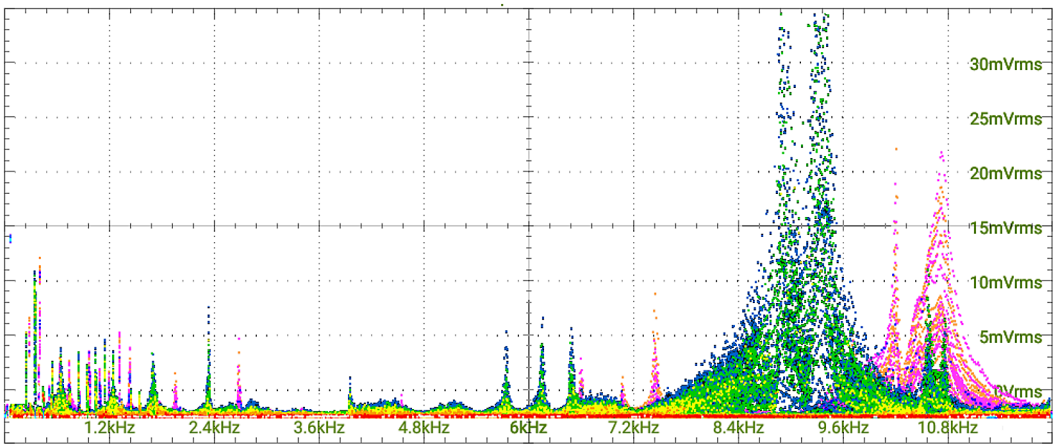

Figure 7. Overlaid spectra of empty cylinder (yellow-pink) and cylinder filled with water (green-blue)

Table 5. Comparison of selected simulated and experimental frequencies

Mode order	SIM freq air (HZ)	EXP freq air (HZ)	ERR air (%)	Sim FR water (HZ)	Exp FR water (HZ)	Err water (%)	Sim FRR (%)	Exp FRR (%)
2ND1	1656.0	1705.9	-2.92	1159.8	1147.5	+1.07	29.96	32.73
3ND1	2276.2	2296.4	-0.88	1715.2	1712.0	+0.19	24.64	25.45
4ND1	3990.7	3945.9	+1.13	3016.9	2905.3	+3.84	24.40	26.37
5ND1	6319.3	6152.3	+2.71	4723.6	NaN	---	25.25	---

approximately 24% to 33% for the lower identified modes (Table 5), are significant and highlight the necessity of considering FSI in the dynamic analysis of such structures.

To provide a deeper understanding of these FSI effects, a comparative modal analysis of the three simulated cases is warranted. The structural modal analysis in vacuum (Table 3, "Modal analysis" columns) establishes a baseline, representing the inherent 'dry' natural frequencies and mode shapes of the glass cylinder, governed solely by its mass and stiffness distribution. These serve as the reference before any fluid interaction.

When a light fluid like air is introduced and coupled acoustically (Table 3, "PS Modal Acoustic AIR" columns), several changes are observed compared to the vacuum case. Firstly, for modes that are primarily structural in nature (e.g., the 2ND1 mode, which appears as MS 5/6 at ~1656 Hz in air versus ~1664 Hz in vacuum), there's a slight frequency reduction. This can be attributed to the minimal added mass effect of air and some degree of acoustic coupling. More significantly, the AIR simulation predicts modes, particularly those with 0ND (axisymmetric/breathing) characteristics (e.g., MS 1, 0ND1 at ~640 Hz; MS 2, 0ND2 at ~850 Hz), which are either absent or occur at vastly different orders in the purely structural vacuum analysis. These are likely acoustic modes of the air cavity within the cylinder, coupled with the structure's vibration. This demonstrates that even a light fluid, when modelled acoustically, alters the system's modal landscape and introduces new, fluid-driven dynamic behaviours. The experimental results for the air-filled case (Table 4) do not clearly capture these purely acoustic air modes, likely due to their low energy, the sensor placement optimized for structural shell modes, and the impact excitation method used.

The introduction of water (Table 3, "PS Modal Acoustic WATER" columns) leads to far more pronounced changes, underscoring its dominant inertial and coupling effects. The most apparent is the substantial frequency reduction for the structural modes (e.g., 2ND1, 3ND1, 4ND1) when compared to both vacuum and air

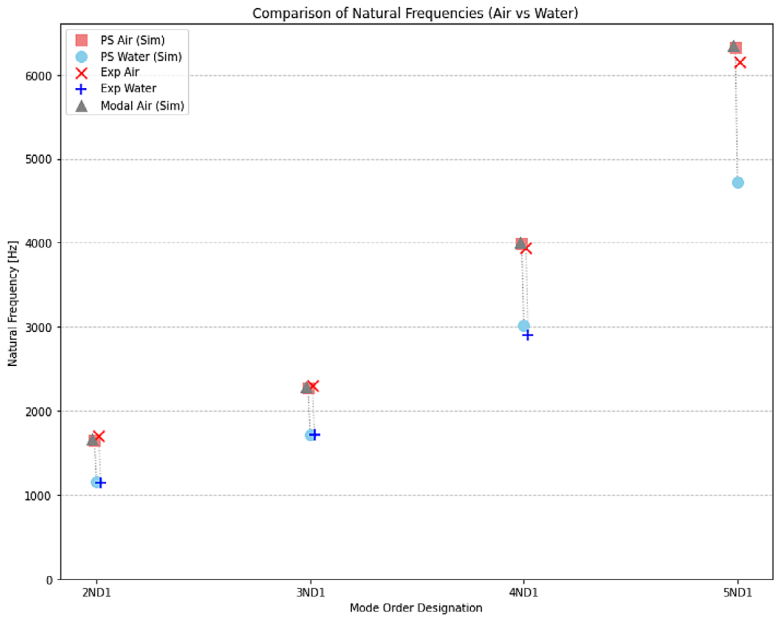

Figure 8. Correlation between experimental and numerical results

simulations. As detailed in Table 5, the FRR due to water for these modes ranges from approximately 24% to 30% in the simulations. This significant reduction directly quantifies the large added mass imparted by the water.

These findings align qualitatively with established theoretical and experimental results for fluid-filled cylindrical shells. Analytical solutions based on potential flow, such as those derived or discussed in the context of Fritz's work [5], predict frequency reductions dependent on fluid density, geometry, and mode shape, which is consistent with observations. Experimental studies on cylinders, like those by Maheri and Severn [7] and Amabili et al. [8], also report substantial frequency decreases due to water loading and emphasize the dependence of the added mass effect on the specific vibration mode. The obtained results, showing varying FRR for different modes (e.g., 2ND1 FRR of ~30% vs. 3ND1/4ND1 FRR of ~24-25% in simulations, Table 5), support this mode-dependency. This variation occurs because the extent to which the fluid is accelerated depends on the specific deformation pattern of the structure for each mode. While a direct quantitative comparison with these specific literature results requires matching geometry and boundary conditions precisely, the trends observed in the study are well-supported.

A critical observation, evident from comparing the mode sequences in Table 3, is the pronounced mode reordering when water is introduced. For instance, in the "PS Modal Acoustic AIR" simulation, the first structural shell mode (2ND1) appears as MS 5/6 around 1656 Hz. In the "PS Modal Acoustic WATER" simulation, this 2ND1 mode is found at MS 2/3 around 1159 Hz, but it is now preceded by a 0ND mode (likely a coupled acoustic-structural mode of the water-filled cylinder) at ~924 Hz. Such reordering indicates that FSI with a dense fluid like water does more than just proportionally scale down all structural frequencies; it fundamentally alters the dynamic characteristics of the coupled system. The sequence of modes changes, and the nature of these modes becomes inherently coupled (vibroacoustic), rather than purely structural or purely acoustic. This implies changes in the mode shapes, which, although not explicitly visualized comparatively for all modes in this study, are indicated by the different modal sequences. The satisfactory agreement between the experimental measurements and the Ansys Modal Acoustics simulations water-filled case provides sufficient confidence in the numerical methodology used to capture these primary FSI effects.

Furthermore, it is important to acknowledge the inherent limitations of this numerical study. The employed linear Modal Acoustics analysis assumes small perturbations and does not account for non-linear phenomena such as cavitation or water detachment, which could occur at high vibration amplitudes (as discussed in the "Water Detachment (Cavitation) & Critical Conditions" section). The model also assumes an ideal fluid (inviscid for the acoustic formulation) and does not consider damping effects from fluid viscosity beyond what might be implicitly handled by radiation boundaries if they were used (not the case here for contained fluid). The material model for the glass is linear elastic, neglecting any potential non-linearities or damage. The boundary conditions, such as the perfectly fixed base and the P = 0 free surface, are idealizations of the real experimental setup. While the P=0 free surface is a common and often adequate approximation for low-frequency vibrations where sloshing is not dominant, it does neglect surface tension and the true impedance of the air above. These idealizations and assumptions, while standard for making the problem computationally tractable and for focusing on the added mass effect, contribute to the observed discrepancies between simulation and experiment, especially for higher or more complex modes.

CONCLUSIONS

This investigation for the first time successfully validated a numerical procedure using Ansys Modal Acoustics for quantifying the water-added mass effect on the vibroacoustic characteristics of a cylindrical container. Key conclusions are:

1. The FEM-based approach accurately predicted natural frequency reductions (24–33% experimentally) due to water loading, with results for primary modes showing good agreement (typically < 4% error) with experimental data.
2. The added mass effect was confirmed to be mode-dependent, with varying frequency reduction rates observed for different nodal diameter modes.
3. Significant mode reordering between air and water simulations was observed, highlighting that FSI with a dense fluid fundamentally alters the coupled system's dynamic

characteristics and mode shapes, beyond a simple frequency scaling.
4. The validated numerical procedure, employing coupled acoustic-structural elements, provides a reliable framework for analysing FSI phenomena in submerged and/or fluid-containing structures.

REFERENCES

1. Chen S.S. Vibration of nuclear fuel bundles. Nucl. Eng. Des. 1975; 35(3): 399–422. https://doi.org/10.1016/0029-5493(75)90071-0
2. Chung H., Chen S.S. Vibration of a group of circular cylinders in a confined fluid. J. Appl. Mech. 1977; 44(2): 213–217. https://doi.org/10.1115/1.3424026
3. Rośkowicz, M., Chachurski, R., Omen, Ł., Jędrak, M. (2025). Analysis of wing in ground-craft water landing. Advances in Science and Technology Research Journal, 19(3), 144–157. https://doi.org/10.12913/22998624/196259
4. Rodriguez C.G., Egusquiza E., Santos I.F., Coussirat M., Valero C. Experimental investigation of added mass effects on a Francis turbine runner in still water. J. Fluids Struct. 2007; 23(6): 887–902. https://doi.org/10.1016/j.jfluidstructs.2006.04.001
5. Cao J., Luo Y., Liu X., Presas A., Deng L., Zhao W., Xia M., Wang Z. Numerical theory and method on the modal behavior of a pump-turbine rotor system considering gyro-effect and added mass effect, Journal of Energy Storage, 2024; 85: 111064, https://doi.org/10.1016/j.est.2024.111064
6. Fritz R.J. The effect of liquids on the dynamic motions of immersed solids. J. Eng. Ind. 1972; 94(1): 167–173. https://doi.org/10.1115/1.3428107
7. Maheri M.R., Severn R.T. Experimental added-mass in modal vibration of cylindrical structures. Eng. Struct. 1992; 14(3): 163–175. https://doi.org/10.1016/0141-0296(92)90027-N
8. Amabili M., Pagnanelli F., Pellegrini M. Experimental investigation of added mass on circular cylindrical shells vibrating in water. Appl. Mech. Mater. 2002; 1–2: 15–22.
9. Ostachowicz W., Krawczuk M., Cartmell M. The location of a concentrated mass on rectangular plates from measurements of natural vibrations. Comput. Struct. 2002; 80(16–17): 1419–1428. https://doi.org/10.1016/S0045-7949(02)00084-6
10. Turek, P., Skoczyński, W. Model research on the influence of bearing preload change on the frequency and form of natural vibrations of the spindle system. Advances in Science and Technology Research Journal, 2020; 14(4), 284–297. https://doi.org/10.12913/22998624/127991
11. Zeng Y., Yao Z., Hong Y., Wang F., Zhang F. Numerical investigation of added mass and hydrodynamic damping on a blunt trailing edge hydrofoil. J. Fluids Eng. 2019; 141(8): 081108. https://doi.org/10.1115/1.4042759
12. Yari E, Ghassemi H. Boundary element method applied to added mass coefficient calculation of the skewed marine propellers. Polish Maritime Research. 2016; (2): 25–31. https://doi.org/10.1515/pomr-2016-0017
13. Rdzanek W.P. Jr, Szemela K. The effect of a concentrated mass on the acoustic power and the resonant frequencies of a circular plate. Arch. Acoust. 2022; 47(4): 529–538. https://doi.org/10.24425/aoa.2022.142895
14. Brandely A., Lefrancois E. A numerical investigation of the added mass effect due to fluid-structure coupling in a rectangular tank – Coupled Problems 2015. In: Schrefler B., Oñate E., Papadrakakis M. (Eds.) Proceedings of the VI International Conference on Computational Methods for Coupled Problems in Science and Engineering. CIMNE, Venice, Italy; 2015: 1058–1071.
15. Urban, O., Pochylý, F., Habán, V. Estimation of added effects and their frequency dependence in various fluid–structure interaction problems. J Braz. Soc. Mech. Sci. Eng. 2024; 46: 631. https://doi.org/10.1007/s40430-024-05175-4
16. Wang W., Zhou L., Xia X., Song X., Wang Z. Numerical study of the natural frequency and mode shape of prototype Francis turbine runner. J. Hydrodyn. 2022; 34(1): 125–134. https://doi.org/10.1007/s42241-022-0013-8
17. ANSYS Theory Reference, Release 2024R1, https://ansyshelp.ansys.com/public/account/secured?returnurl=/Views/Secured/corp/v242/en/ans_thry/ans_thry.html